Identifying unknown nanocrystals by fringe fingerprinting in two dimensions & free-access crystallographic databases

Peter Moeck*[1], Ondřej Čertík[1,2], Bjoern Seipel[1], Rebecca Groebner[1], Lori Noice[1], Girish Upreti[1], Philip Fraundorf[3], Rolf Erni[4], Nigel D. Browning[4,5], Andreas Kiesow[6], and Jean-Pierre Jolivet[7]
[1] Department of Physics, Portland State University, P.O. Box 751, Portland, OR 97207-0751, USA

[2] Faculty of Mathematics and Physics, Charles University of Prague, Ke Karlovu 3, 121 16 Praha, The Czech Republic

[3] Department of Physics and Astronomy and Center for Molecular Electronics, University of Missouri at St. Louis, MO 53121, USA

[4] Department of Chemical Engineering and Materials Science, University of California at Davis, One Shields Avenue, Davis, CA 95616, USA; now at: FEI Electron Optics, PO Box 80066, 5600 KA, Eindhoven, The Netherlands

[5] National Center for Electron Microscopy, MS 72-150, Lawrence Berkeley National Laboratory, 1 Cyclotron Road, Berkeley, CA 94720, USA

[6] Fraunhofer Institute for Mechanics of Materials, Heideallee 19, 06120 Halle, Federal Republic of Germany

[7] Department of Condensed Matter Chemistry, University Pierre and Marie Curie, 4 place Jussieu (T54-E5), 75252 Paris, Cedex 05, France

ABSTRACT

New needs in determining the crystallography of nanocrystals arise with the advent of science and engineering on the nanometer scale. Direct space high-resolution phase-contrast transmission electron microscopy (HRTEM) and atomic resolution Z-contrast scanning TEM (Z-STEM), when combined with tools for image-based nanocrystallography possess the capacity to meet these needs. This paper introduces such a tool, i.e. fringe fingerprinting in two dimensions (2D), for the identification of unknown nanocrystal phases and compares this method briefly to qualitative standard powder X-ray diffractometry (i.e. spatial frequency fingerprinting). Free-access crystallographic databases are also discussed because the whole fingerprinting concept is only viable if there are comprehensive databases to support the identification of an unknown nanocrystal phase. This discussion provides the rationale for our ongoing development of a dedicated free-access Nano-Crystallography Database (NCD) that contains comprehensive information on both nanocrystal structures and morphologies. The current status of the NCD project and plans for its future developments are briefly outlined. Although feasible in contemporary HRTEMs and Z-STEMs, fringe fingerprinting in 2D (and image-based nanocrystallography in general) will become much more viable with the increased availability of aberration-corrected transmission electron microscopes. When the image acquisition and interpretation are, in addition, automated in such microscopes, fringe fingerprinting in 2D will be able to compete with powder X-ray diffraction for the identification of unknown nanocrystal phases on a routine basis. Since it possesses a range of advantages over powder X-ray diffractometry, e.g., fringe fingerprint plots contain much more information for the identification of an unknown crystal phase, fringe fingerprinting in 2D may then capture a significant part of the nanocrystal metrology market.

Keywords: nanocrystallography, nanometrology, transmission electron microscopy, nano-crystallography database

Two- and Three-Dimensional Methods for Inspection and Metrology III, edited by Kevin G. Harding,
Proc. of SPIE Vol. 6000, 60000M, (2005) · 0277-786X/05/$15 · doi: 10.1117/12.62918

1. INTRODUCTION

The market for nanomaterials is expected to rise from $900 million in 2005 to $11 billion in 2010[1]. The impact of nanomaterials will be larger than their immediate total material value and is estimated to be over $340 billion in 2010[2]. As any technology requires its own specific metrology, nanomaterials science and engineering need nanometrology in order to result in industrial products.

Classical (i.e. non-aberration corrected) transmission electron microscopy[3,4] (TEM) and scanning TEM[5,6] traditionally provide structural, chemical, and morphological information for thin crystals. Non-aberration corrected medium acceleration voltage (200 - 400 kV) HRTEM[4] and Z-STEM[5,6] provide 2D projections of the 3D electrostatic potential energy distribution within crystals with a directly interpretable spatial resolution in the range of 0.2 - 0.136 nm. The latter spatial resolution (0.136 nm) is frequently demonstrated on {004} Si "dumbbells" in <110> orientations[6] and the former (0.2 nm) is being considered as the point(-to-point or Scherzer) resolution limit from which on a TEM may be considered to constitute a dedicated phase-contrast HRTEM[4].

The Scherzer resolution is commonly defined as $\approx 0.7\sqrt[4]{C_s\lambda^3}$, where λ is the electron wavelength and C_s is the spherical aberration coefficient of the objective lens. (Although the resolution of a TEM is specimen dependent when the object is crystalline, we will for simplicity use below the point resolution of the instrument as defined above by Scherzer's formulae.) Especially for non-aberration corrected TEMs with field emission guns, the information limit (which is determined by the overall stability of a microscope) can be much smaller than the Scherzer resolution and is given by the inverse of the maximally transferred spatial frequency, g_{max}.

Due to the tiny size of nanocrystals, well established electron crystallography characterization methods that are based on dynamic electron scattering effects, such as convergent beam electron diffraction with 100 to 400 kV electrons (CBED), can not satisfy the above mentioned need. This is because the CBED disks are largely devoid of their fine structure[3], which made them so useful for crystallographic analyses, when the nanocrystal diameter is on the order of 10 nm. Image-based nanocrystallography[7-15], on the other hand, requires kinematical electron scattering conditions and, therefore, works well for nanocrystals.

For both conceptual and practical reasons, we typically restrict the application of image-based nanocrystallography tools to the point resolution of the microscope. In standard phase-contrast HRTEM, this resolution is defined as the reciprocal value of the crossover of the contrast transfer function at the Scherzer (de)focus ($-\sqrt{\lambda C_s}$) of the microscope.

At this resolution, electron phase contrast images of weak-phase objects[16] or pseudo-weak-phase objects[17] can be considered to constitute projections of the electrostatic potential of the transmitted crystal, the imaging process is essentially linear, and the electrons scatter essentially kinematically, resulting in a directly interpretable structure image. For specimens of medium atomic weight and medium acceleration voltages, structure images with the correct positions and spacings of the atoms, but not the correct intensity of both heavier and lighter atoms, may be obtained for sample thicknesses of up to several nm.[18]

If not removed by the objective aperture in contemporary (non-aberration corrected) HRTEM, spatial frequencies larger than the reciprocal value of the point resolution of the microscope may be present in the image, but are not reliably transferred (i.e. can be absent) since the contrast transfer function oscillates beyond this resolution (resulting in zero contrast transfers at several spatial frequencies). The information beyond this resolution is, in addition, delocalized and complicates the image interpretation. Hence, we typically exclude it conceptually and practically by the application of an objective aperture of $\sqrt{2}\sqrt[4]{\lambda/C_s}$ rad.

Then the objective aperture restriction ensures that the HRTEM image-based nanocrystallographic analyses which employ tools such as the one reviewed in this paper, give reliable results that are readily and directly interpretable. Similarly, in Z-STEM imaging, the point(-to-point) resolution is that where the projection of the electrostatic potential of the sample is convoluted with the so called "Scherzer electron probe". Thicker nanocrystals can reliably be analysed here without a contrast reversal in the image, because the imagining process is essentially incoherent. In addition, there is chemical contrast proportional to approximately the square of the atomic number in Z-STEM images.

In the first part of this paper, we introduce the concept of fringe fingerprinting[7-11] in 2D and present theoretical fringe fingerprint plots of several nanocrystal ensembles (i.e. gold, α-manganese, barium, silicon, atomically ordered CuAu, and two of the titania polymorphs) in their most basic form. At the end of the first part of this paper, fringe fingerprinting in 2D is briefly compared to standard qualitative powder X-ray diffractometry (i.e. spatial frequency fingerprinting). Crystallographic databases are discussed in the second part of this paper because the whole fingerprinting concept is only viable if there are comprehensive databases that support the identification of an unknown nanocrystal phase. This discussion provides the rationale for our ongoing development of a dedicated Nano-

Crystallography Database (NCD) that will contain comprehensive information on both nanocrystal structures and typical morphologies. The current status of the NCD project and plans for its future developments are briefly discussed at the end of the second part of this paper.

The word fringe is typically used in physics for any periodic light or dark band produced by diffraction, scattering, or interference of electromagnetic or matter waves. We use fringe here for periodic contrast variations in HRTEM or Z-STEM images (and are not interested in the intensity of HRTEM fringes). For structures where there is just one atom at a lattice point, fringes are also lattice fringes within the crystallographic definition of a lattice. For structure where there is more than one atom at a lattice point, fringes are the projections of crystallographic planes on which atoms reside.

The super-linearly increased viability of image-based nanocrystallography in (either) 2D (or 3D) with improved directly interpretable point resolution[8,12-15] around 0.1 nm (as nowadays routinely obtainable by spherical aberration corrected objective lenses[19-26]) and well below 0.1 nm (as prospectively obtainable by combining spherical aberration corrected objective lenses with either electron gun monochromatization, in-column electron energy filtering, or chromatic aberration correction) will be demonstrated briefly in the final part of this paper on sub-stoichiometric WC_{1-x} nanocrystal ensembles.

2. FRINGE FINGERPRINTING IN TWO DIMENSIONS

As a high-resolution conceptual extension to certain aspects of variable coherence microscopy[27] and fluctuation microscopy[28], fringe fingerprinting in 2D was recently proposed by Philip Fraundorf and co-workers.[7-11] Angular covariance plots, which may also be called "fringe fingerprint plots", represent in their most basic form a plot of visible interfringe angles of crossed fringes versus the respective reciprocal lattice spacings of these fringes. Analyzing a single Au nanocrystal in a femto-laser treated gold-polymer nanocomposite[29] in HRTEM mode, Figs. 1a and 1b, with a microscope that possesses a point resolution of 0.19 nm, the experimental fringe fingerprint plot shown in Fig. 2a was obtained. While for cross-fringes with different spacings, there are two data points in fringe fingerprint plots, the crossing of two symmetrically related fringes (which possess by symmetry the same spacing) results in just one data point, see annotation in Fig. 2b.

Below we show examples of theoretical fringe fingerprint plots for ensembles of gold, α-manganese, barium, silicon, atomically ordered CuAu, and polymorph titania nanocrystals in their most basic form for a range of point resolutions, Figs. 2b, 3a,b, 4a-d, and 5a,b. As mentioned above, the criterion for a fringe being visible here is that its spatial frequency is reliably transferred to the HRTEM or Z-STEM image, i.e. that its fringe spacing is larger than the point resolution of the microscope. Comparing Fig. 2b with Figs. 3a and 3b, i.e. fringe fingerprint plots for the same nanocrystals with increasing point resolutions, it is obvious that fringe fingerprint plots become significantly more "characteristic" with improved point resolution. By "characteristic" we mean both the total sum of information in a fringe fingerprint plot and where exactly the individual data points are located. Fringe fingerprint plots also contain space group information such as the "signatures" of translation lattice types, glide planes, and screw axes in projection.

Because all possible interfringe angles are the same for all cubic crystals, space group information, can, as a matter of principle, be derived from their fringe fingerprint plots. The presence or absence of data points in a fringe fingerprint plot of a cubic crystal is, therefore, characteristic of its translation symmetry. Primitive space groups without screw axes and glide planes possess for example no "systematic absences" in fringe fingerprint plots. Since the systematic elucidation of this idea is rather complex, we will deal with it elsewhere and present here with Fig. 3a and Figs. 4a-c only illustrations of this idea. For convenience, point resolutions have been chosen for each of these four fringe fingerprint plots that result in just the first three reciprocal lattice spacings being given in each plot.

A comparison of Fig. 3a with Fig. 4d, i.e. two plots for the same point resolution for nanocrystals that have 50 % of their atoms in common, reveals an effect of atomic ordering in alloys with the face centered cubic crystal structure (e.g. Au and Cu) on fringe fingerprint plots. It is obvious that the atomically ordered CuAu phase (Fig. 4d) possesses, due to its lower symmetry, a more characteristic fringe fingerprint plot than Au (Fig. 3a). Figs. 5a and 5b, finally, show fringe fingerprint plots for the two titania polymorphs rutile and brookite. Again the lower symmetric brookite possesses, for the same point resolution of the microscope, the more characteristic fringe fingerprint plot. (Note that the unit cell of brookite is also much larger).

More elaborate fringe fingerprint plots than those given in Figs. 2b, 3a,b, 4a-d, and 5a,b may contain in the third dimension histograms of the probability of seeing crossed fringes in an ensemble of nanocrystals. The equations for calculating such probabilities for an ensemble of randomly oriented nanocrystals are given in ref.[7]. From these equations, it is also possible to calculate the tilt range over which any cross-fringe will be visible for a particular nanocrystal thickness. This allows on the experimental level for both the determination of the nanocrystal thickness[30]

and a strategy for collecting more experimental data for fringe fingerprinting in 2D. One simply tilts an ensemble of nanocrystals in random directions by several degrees in order to record more images that show crossed fringes.
Another type of more elaborate fringe fingerprint plots may contain the angular and spatial frequency ranges over which the fringe crossings/zone axes are visible. These ranges will be functions of the nanocrystal thicknesses. Foreshortening projection effects, e.g. fringe spacings appearing shrunk by a factor of cos γ in the direction perpendicular to the tilt axis, will be larger the smaller the nanocrystals are. This is because fringe crossings/zone axes will be visible over a wider angular range (γ) for smaller nanocrystals, as can be calculated from the equations given in ref.[7].

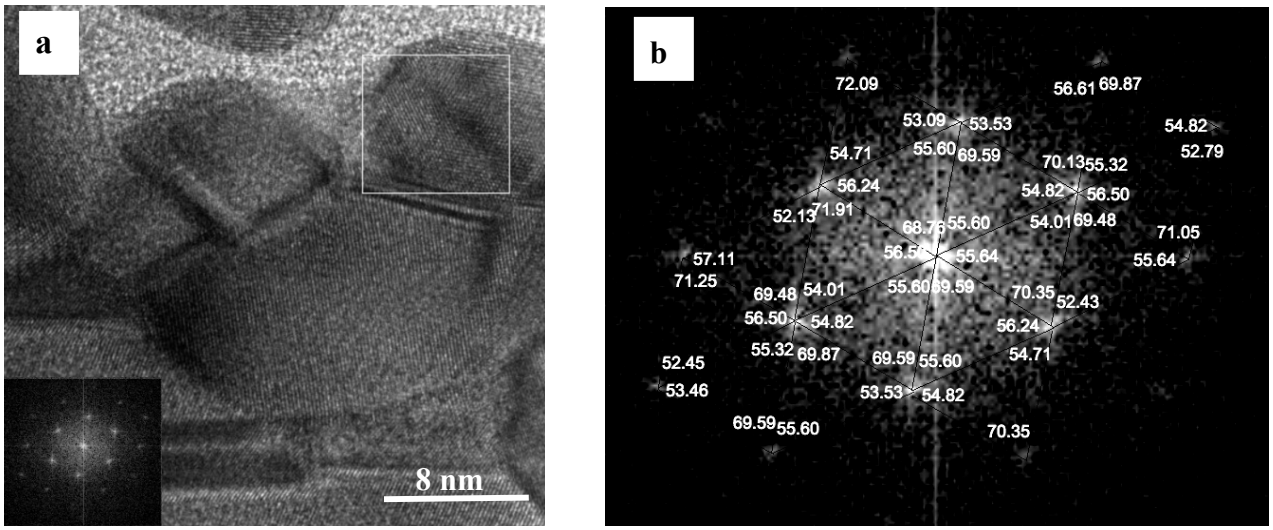

Figure 1: Experimental images for fringe fingerprinting of a femto-laser treated **gold** nanocrystal in a gold-polymer nanocomposite.[29] The nanocrystal orientation is close to the <110> zone axis. The 200 kV FEI Tecnai G^2 F20 UT microscope at the National Center for Electron Microscopy, Lawrence Berkeley National Laboratory, with a point resolution of 0.19 nm was employed. **(a)** phase-contrast image where the inset is the Fourier transform power spectrum of the marked area; **(b)** magnified Fourier transform power spectrum of the 64 nm^2 inset from (a) with measured interfringe angles. The faint dark lines are guides for the eye.

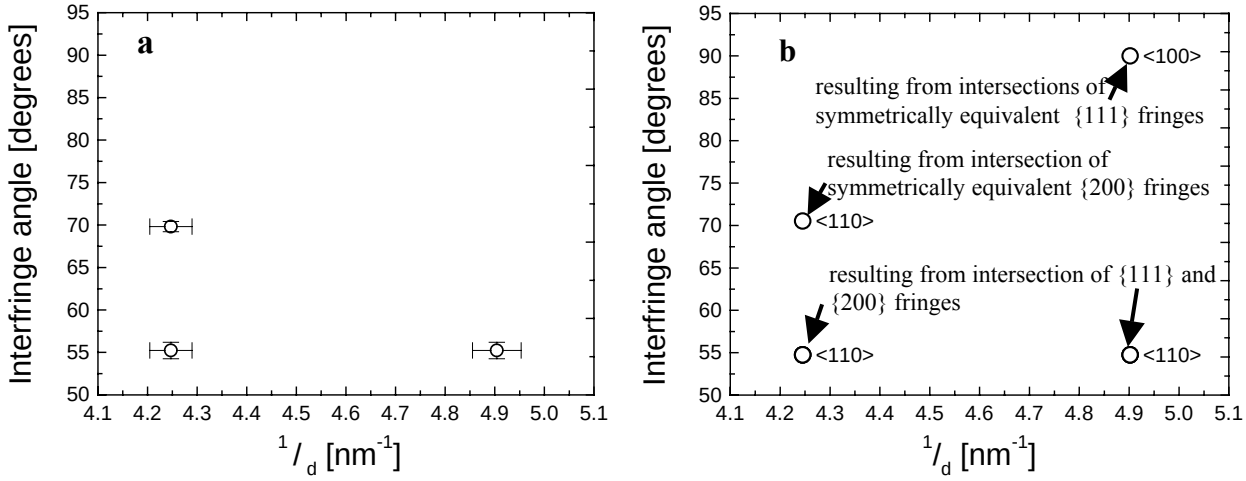

Figure 2: (a) Experimental fringe fingerprint plot for the **gold** nanocrystal that is marked in Fig. 1a. Data that are shown in Fig. 1b were used to derive this plot. The large error bars on the special frequency measurements are due to the preliminary nature of this investigation[♣]; **(b)** Basic theoretical fringe fingerprint plot for **gold**, space group Fm$\bar{3}$m, a = 0.408 nm, point resolution 0.19 nm. The theoretical data points (open circles) are explained by annotations and pointed to by arrows. For simplicity we plotted only intersection angles that are smaller than or equal to 90°. A fringe fingerprint plot for the complementary angles, i.e. angles equal to or larger than 90° has essentially the same information content.

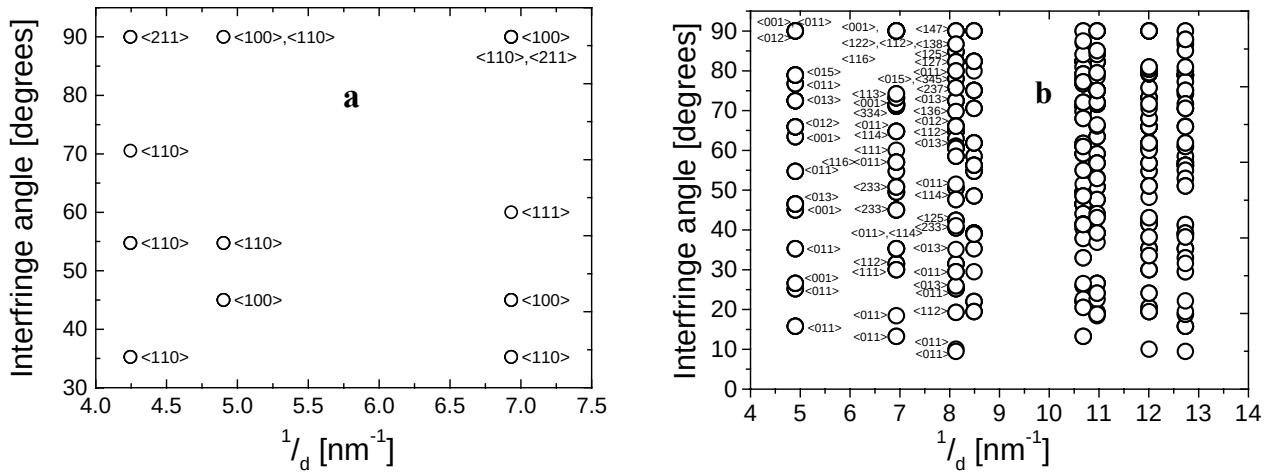

Figure 3: Basic theoretical fringe fingerprint plot for **(a) gold**, space group $Fm\bar{3}m$, a = 0.408 nm, point resolution 0.14 nm (as obtainable in Z-contrast STEM mode with the FEI Tecnai G^2 F20 UT microscope at the National Center for Electron Microscopy in Berkeley); **(b)** point resolution 0.07 nm (as obtainable in high resolution phase contrast mode with a C_s-corrected FEI Titan 80-300 microscope), only the first three columns of data points are indexed as they are clustering strongly for higher spatial frequencies.

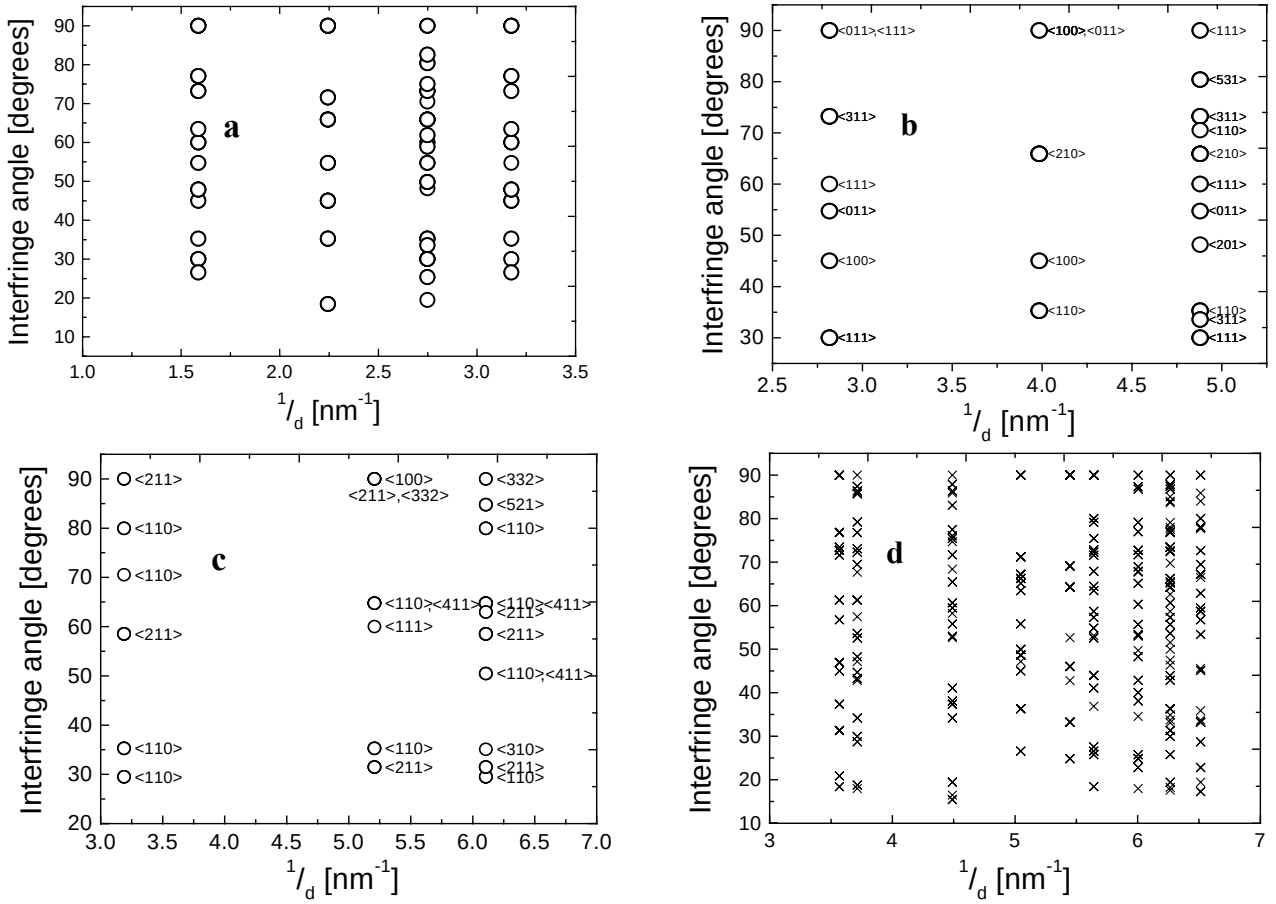

Figure 4: Basic theoretical fringe fingerprint plot for **(a) α-manganese**, space group $I\bar{4}3m$, a = 0.891 nm, point resolution 0.3 nm; **(b) barium**, space group $Im\bar{3}m$, a = 0.501 nm, point resolution 0.19 nm; **(c) silicon**, space group $Fd\bar{3}m$, a = 0.543 nm, point resolution 0.16 nm; **(d) CuAu**(-I) (tetragonal, $^c/_a \approx 0.93$ for order parameter $\eta \approx 1$), i.e. the (001) atomically ordered solid solution in this material system, space group P 4/mmm, a = 0.396 nm, c = 0.367 nm, point resolution 0.14 nm.

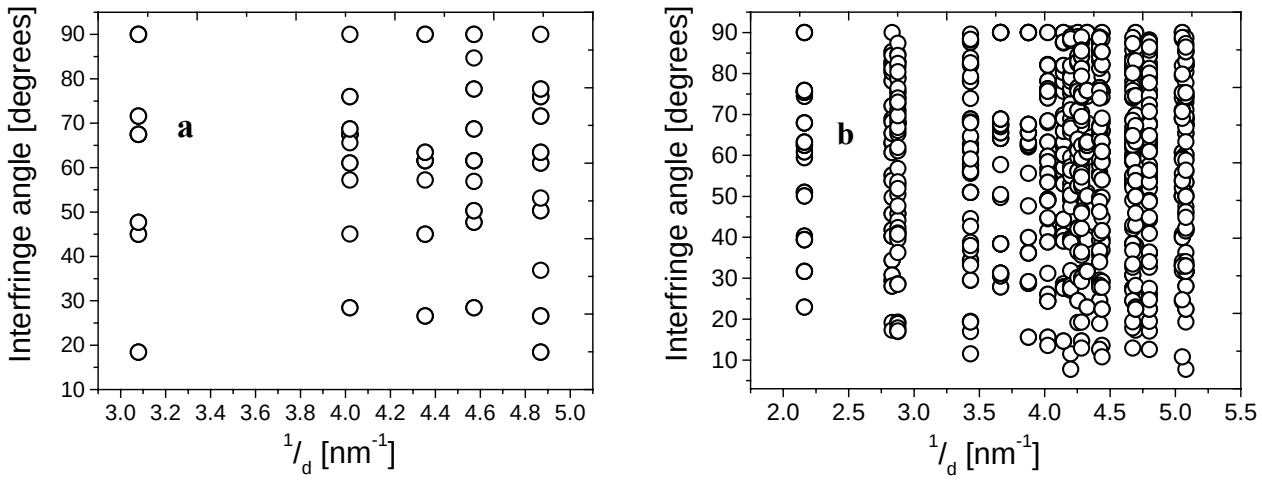

Figure 5: Basic theoretical fringe fingerprint plot for the titania polymorphs **(a) rutile**, space group P 4_2/mnm, a = 0.459 nm, c = 0.296 nm; **(b) brookite**, space group P bca, a = 0.918 nm, b = 0.546 nm, c = 0.514 nm; both for point resolution 0.19 nm.

Although fringe-spacing projection foreshortening effects are rather small (e.g. misorientations of up to 5° would result in a foreshortening factor range of 0.9962 to 1 depending on the direction of the fringe spacing with respect to the tilt axis), more elaborate fringe fingerprint plots could incorporate such effects. Similarly, interfringe (and interfacial) angle projection foreshortening effects can be incorporated in more elaborate fringe fingerprint plots (or readily corrected for[31]). Systematic experimental errors in fringe fingerprinting are due to frequently observed nanocrystal shape anisotropies.[32] Fortunately, these errors are typically small in comparison to random measurement errors♣, so that they can frequently be neglected.

The utility of basic and more advanced theoretical fringe fingerprint plots is founded in them being a rather specific characteristic for an ensemble of nanocrystals against which experimental data from HRTEM or Z-STEM images can be directly compared for the identification of unknown nanocrystal phases. Although somewhat different in their information content♣♣, basic and more advanced fringe fingerprint plots are in their outlay similar to powder X-ray (or electron) diffractograms, where scattered intensity (or the probability of detecting scattered electrons or X-ray photons) is plotted on the ordinate and two times the corresponding scattering angle and/or spatial frequency is plotted on the abscissa(s), Fig. 6.

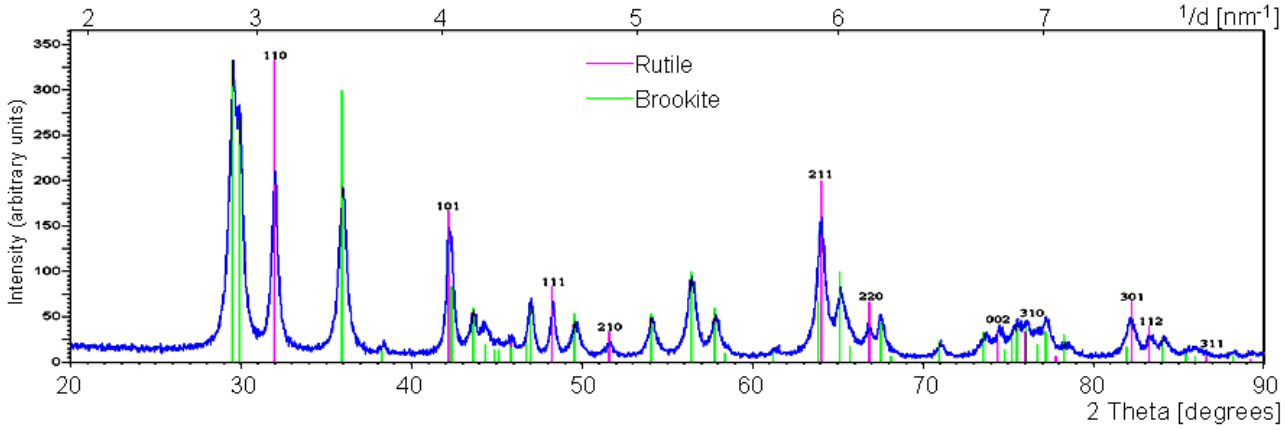

Figure 6: Experimental powder X-ray diffraction curve (scattered X-ray intensity or X-ray photon counts in the detector versus two times scattering angle on the bottom abscissa, scattered intensity versus spatial frequency on the top abscissa) of a mixture of rutile and brookite nanocrystals[33], Co $K\alpha_{1/2}$ radiation, the peaks are marked on the basis of the well known Powder Diffraction File database. Most of the peaks of the rutile phase are indexed.

It has been said that powder diffractograms/spatial frequency plots represent "two-dimensional data"[34], i.e. scattered intensities and magnitudes of lattice spacings. The first of these "dimensions" depends partly on the experiment and the second is characteristic to the phase of the unknown crystal, i.e. experiment independent. Obviously, with respect to

"diffractometry fingerprint plots" such as Fig. 6, already the most basic fringe fingerprint plots, Figs. 2b, 3a,b, 4a-d, and 5a,b, which do not contain information on experiments, possesses "extra dimensions" that are characteristic to the unknown crystal phase. These "extra dimensions" are the magnitudes of any acute angles between any two crossing reciprocal lattice vectors and information on the magnitudes of any two reciprocal lattice vectors that cross each other. When compared (in the same spatial frequency range*** to powder diffractograms), fringe fingerprint plots, thus, contain much more crystal structure specific information for the unique identification of nanocrystals. Moreover, image-based nanocrystallography in 2D delivers morphological information in addition to structural information.
Since the basic idea of fingerprinting is that all one needs to do in order to identify some unknown object is collect characteristic information from the object and compare this information with the information that is stored in a comprehensive data base, we discuss free-access crystallographic database for the identification of unknown crystal phases in the following section. This discussion will show that there is a need to develop a dedicated database with "nanocrystal specific information" to support both fringe fingerprinting in 2D and image-based nanocrystallography in general.

3. FREE-ACCEESS CRYSTALLOGRAPHIC DATABASES

Fifteen years after the development of the World Wide Web, there is already a variety of internet based free-access crystallographic databases. In this part of the paper we discuss the subset of free-access databases that deals with inorganic crystals. Only those databases are discussed that offer unrestricted and anonymous access.
The database MINCRYST[35] is maintained and hosted by the Russian Academy of Sciences and contains more than 6,000 entries for minerals from which X-ray powder diffractograms can be calculated on the fly. 3D visualizations of the entries are provided by means of the java-based freeware program "Jmol".[36] The Naval Research Laboratory's Center for Computational Materials Science provides an on-line database for education and research support under the name "Crystal Lattice Structures".[37] Currently this database contains 254 entries in 90 space groups. 3D visualizations of the entries are also provided by Jmol[36] applets. In both of these databases, files can neither be downloaded nor uploaded by the general public. The "Reciprocal Net"[38] is a distributed database of molecular structures and its main web site is hosted at Indiana University at Bloomington. Crystallographic Information Files**** (CIFs), e.g. Fig. 7a, for approximately 400 common molecules (and crystal structures) are downloadable by the general public. 3D visualizations of these common molecules (and crystal structures) are provided by a range of Java based applets.
The on-line American Mineralogist Crystal Structure Database (AMCSD) was erected in 2003 and contains more than 8,000 critically evaluated entries.[39,40] Files can be downloaded from this database in CIF format. A range of PC based freeware programs for, e.g., the visualization of crystal structures (XtalDraw) and for the calculation of powder X-ray and neutron diffractograms (XPow), is available for downloading from the AMCSD site at ref.[41]. The database is maintained under the care of both the Mineralogical Society of America and the Mineralogical Association of Canada.
Ref.[39] states that approximately 75 % of the manuscripts that were submitted to the journals "American Mineralogist" and "Canadian Mineralogist" possess errors of one sort or another. For comparison, ref.[42] states that about 40 % of the CIFs submitted for inclusion into the commercial Cambridge Structural Database contain errors that arise mainly from the manual editing of these files by their authors. The critical evaluation of data to be included in a crystallographic database is, therefore, a major concern for both commercial and free-access databases. This might be one of the reasons that no provisions for uploading data to the AMCSD are provided.
Records of approximately 31,000 full crystal structure determinations in the form of CIFs are freely accessible on line at the Crystallography Open Database (COD).[43,44] This data base was also started in 2003 and is rapidly growing as more and more crystallographers and scientific institutes/societies/academies donate their collections of CIFs and upload them over the internet so that anybody with access to the World Wide Web can access them. The COD also contains all the data sets that are in the AMCSD. The long term objectives of the COD initiators are summarized on their web page[44] as: (*i*) providing free access to comprehensive crystallographic data (including the atomic coordinates) on all known inorganic, metallic, organometallic, and organic crystalline compounds and (*ii*) complementing the existing commercial databases (which typically specialize on only one or two classes of crystals and contain in addition to crystallographic information a range of physical properties). Another major concern of the COD initiators is supporting crystallographers in emerging countries.
By providing the opportunity to check rapidly and early on in an investigation (i.e. already after the cell parameters have been determined) if the structure of the particular crystal under investigation has already been solved, the COD also helps increasing the productivity of structure determinations. To insure a high quality of the data entries, the policy

of the COD is that only those CIFs that result from structure refinement software can be uploaded. Over the main web page of the COD[44], a subset database of more than 1,500 entries of predicted crystal structures is accessible under the acronym PCOD for "predicted COD". The PCOD database allows for the visualization of polyhedra or wire frames employing the free program "CosmoPlayer".[45]

As a complementary project with a similar philosophy to both the COD and the AMCSD, the nanocrystallography group at Portland State University started in 2005 the Nano-Crystallography Database (NCD) project.[46] Since both structure and morphology of nanocrystals are crucial to their physical properties, the NCD will be collecting entries on both the full structures (including atomic coordinates) and the typical morphologies of inorganic crystals in the form of CIFs. The information on the typical crystal morphologies for nearly 1,300 phases that are collected in the "Bestimmungstabellen für Kristalle"[47] will be the first to be included in the NCD. Because many electron microscopists work on rather simple inorganic structures, we will write and upload CIFs to support their work. A good starting point for this are the descriptions of the 161 full structure determinations (i.e. atomic coordinates, space group, and unit cell parameters) in the second edition of Wyckoff's classical reference book "Structure of Crystals".[48] To insure a high quality of the data entries, we provide a comprehensive on-line syntax check for CIFs.[49] The International Union of Crystallography also provides a complimentary on-line check of CIFs.[50] Only those CIFs that pass both tests will be uploaded to the NCD.

The NCD is being developed to support image-based nanocrystallography, i.e. methods that determine ideal and real structures and morphologies of nanocrystals from transmission electron microscopy images, in general. This is because after an ensemble of nanocrystals is for example fingerprinted in 2D and the crystal phase identified, the electron microscopist may like to index the faces of the nanocrystals, derive the tracht, and give a description of the habit. Visualizations of the entries in the NCD in three dimensions are, therefore, crucial. For a start, we provide 3D visualizations by means of Jmol[36] applets for the structural information[49] that is contained in the entries of the COD, Figs. 7b, and 8. Next we will work on providing 3D visualizations of the morphological information that will be contained in the entries of the NCD. We plan to use the program "XMorph"[51] for the latter purpose.

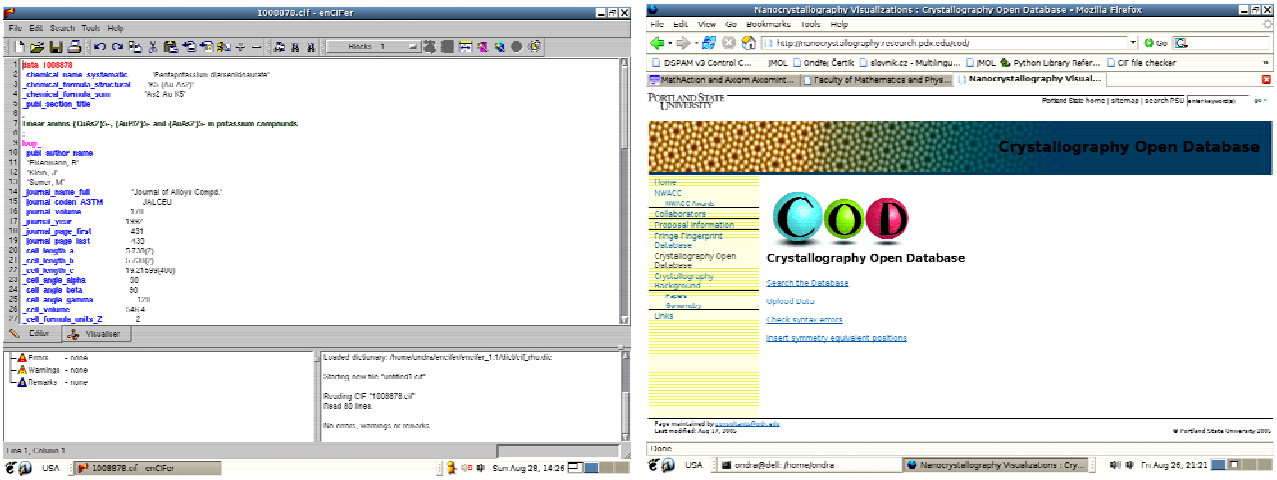

Fig. 7: Screenshots of **(a, left)** the Crystallographic Information File (CIF) of As_2AuK_5, displayed by the free program "enCIFer" ♣♣♣♣♣; **(b, right)** the opening screen of the website that facilitates the free accesses to our local version of the Crystallography Open Database (COD). Searching this database for the simultaneous presence of Au and K in a structure results currently in 6 entries of which the As_2AuK_5 structure is displayed in Fig. 8.

Fig. 8 shows the 3D visualization of one unit cell of the As_2AuK_5 structure in Jmol. As with any Jmol[36] applet, one can zoom into the display of the atomic arrangement. A range of tools that allow, for example, for the measurement of distances between atoms or the bond angles between three atoms, are also provided. The actual visualization of a COD database entry in three dimensions is facilitated by turning the displayed atomic arrangement, e.g. Fig. 8, around three mutually perpendicular axes.

We are also writing software that calculates basic and more elaborate theoretical fringe fingerprint plots on the fly for the entries in the NCD for arbitrary directly interpretable image resolutions. A wide range of help files will clarify core crystallographic concepts so that the NCD can also be used for class room instructions, self study on structures and morphologies of nanocrystals, and other educational purposes.

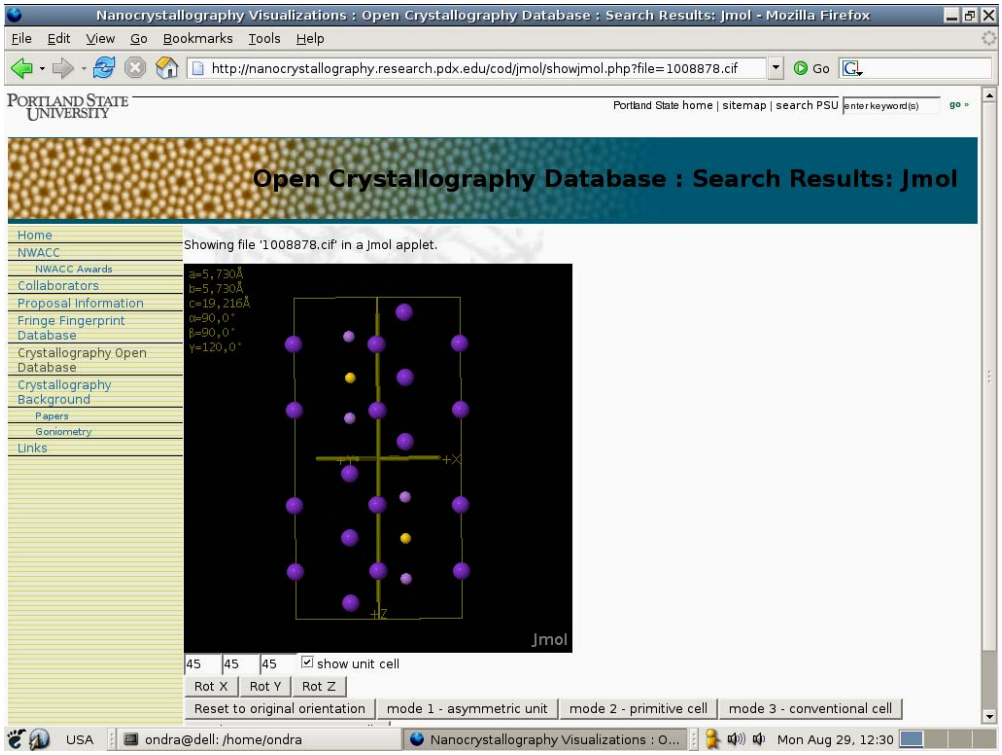

Figure 8: Screenshot of the visualization of one unit cell of the As_2AuK_5 structure[49] (also a record of a moment in time - Monday August 29, 12:30 - of the development of the NCD[46]).

4. VIABILITY OF IMAGE-BASED NANOCRSTALLOGRAPHY

As Figs. 1a,b and 2a,b demonstrate, image-based nanocrystallography by means of fringe fingerprinting in 2D is possible with the current generation of TEMs. It will, however, be much more viable in aberration-corrected TEMs, see Table 1 and refs.[8,12,13]. (Being able to see and analyze more reciprocal and direct lattice vectors in the same unit of orientation space also lessens the necessary angular range of the specimen goniometer for the application of other image-based nanocrystallography tools such as fringe fingerprinting in 3D and transmission electron goniometry.[8,14,15]) Note that when the spherical aberration of the objective lens of a TEM is reduced to zero, directly interpretable (amplitude contrast) structure images, which arise from electron channelling, become possible[19]. For a C_s on the order of 50 µm (when a CEOS spherical aberration corrector is retrofitted to a FEI/Philips CM 200 FEG ST), directly interpretable phase-contrast structure images with minimized contrast delocalisations are also possible.[19] It is such images which are required with preference for other branches of image-based nanocrystallography, e.g. discrete atomic resolution tomography[52] and transmission electron goniometry when the shape of a nanocrystal is to be elucidated. For $C_s = 16/3\lambda^3 g_{\max}^4$, the resolution of an aberration-corrected TEM is equal to the information limit of the microscope.[19]

With FEI company's Titan 80-300 microscope[25,26], a C_s of a few µm is readily obtained by means of extensive computer support (even at an industrial exhibition hall at an international conference![53]), and both the Scherzer and the Lichte (de)focus are on a routine basis nearly indistinguishable from the Gauss focus. As long as the nanocrystals are thin enough to approximate reasonably well to weak phase objects, directly interpretable structure projections of the electrostatic potential of the transmitted crystals can be readily obtained with this new generation of TEMs, Table 1.
When the image acquisition and interpretation in such a microscope are in addition automated, fringe fingerprinting in 2D will become so fast that it can compete on a routine basis with qualitative X-ray powder diffraction for the identification of unknown nanocrystal phases. It may then capture a significant part of the nanocrystal metrology market, which can be forecast to be in the billions of dollars range (as implied by the first two sentences of the introduction to this paper).

Directly interpretable image resolution [nm]	Spherical aberration coefficient C_S of objective lens [mm], FEI Co. microscope example (objective lens type)	Total number of resolved lattice plane spacings (magnitudes of reciprocal lattice vectors) and their indices types within the stereographic triangle [001]-[011]-[111]	Total number of visible zone axes (lattice fringe crosses, projections of direct lattice vectors) and their indices within the stereographic triangle [001]-[011]-[111]
0.19	0.5, Tecnai F20 UT (Ultra Twin lens)	2, i.e. {111}, {200}	2, i.e. [001], [011]
0.12	≈ 0, Tecnai F20 ST with C_S corrector (Super Twin lens)	2^3, i.e. {111}, {200}, {220}, {311}	2^3, i.e. [001], [011], [111], [112], [013], [114], [125], [233]
0.07	≈ 0, Titan 80-300 with C_S corrector (Super Twin lens)	> 2^4, i.e. {111}, {200}, {220}, {311}, {331}, {420}, {422}, {511}, {531}, {442}	> 2^4, but highly indexed zone axes are less characteristic

Table 1: Total number of resolved lattice plane spacings and visible zone axes as a function of directly interpretable image resolution for sub-stoichiometric WC_{1-x} nanocrystals. Spherical aberration coefficients for three state-of-the-art TEMs from FEI Company with these point resolutions are also given. When we take, in a purely phenomenological manner, the total number of resolved lattice plane spacings in one stereographic triangle, third column, as measure of the feasibility of fringe fingerprinting in 2D, there is a strongly super-linear increase in feasibility with improvements in directly interpretable image resolution. (Even for crystals with small lattice constant such as Au, Fig. 3b, or WC_{1-x}, the data points in fringe fingerprint plots have a strong tendency to cluster when lattice spacings below 0.1 nm are resolved. Because of this clustering, these data points are less characteristic for fringe fingerprinting purposes to identify unknown nanocrystals.)

CONCLUSIONS

Fringe fingerprinting in two dimensions is experimentally feasible and possesses for nanocrystals a range of advantages over standard powder X-ray diffractometry. As for any kind of fingerprinting, the method needs support from a comprehensive database of previously collected or calculated fingerprints. Since such a novel database shall support image-based nanocrystallography in general, it will also contain morphological information. In short, a dedicated Nano-Crystallography Database (NCD) is in the process of being erected on the basis of the Crystallography Open Database (COD), sharing the COD's philosophy of free access for everyone over the internet. Visualizations in three dimensions of both the nanocrystal structure and morphology will be integral parts of the NCD. Since the NCD will be mainly used by the transmission electron microscopy community, we will make sure that over time most of the predominantly inorganic nanocrystals this community is working on become part of this database. Although feasible with the current generation of TEMs, fringe fingerprinting in two dimensions (and image-based nanocrystallography in general) will become much more viable in future aberration-corrected transmission electron microscopes.

ACKNOWLEDGMENTS

This research was supported by an award from Research Corporation and a grant by the National Center for Electron Microscopy (NCEM), Lawrence Berkeley National Laboratory. Additional support was provided by the NorthWest Academic Computing Consortium and Portland State University. We are grateful to both Prof. Armel Le Bail from the Université du Maine and Dr. Christian Kisielowski from the NCEM for comments on this paper.

REFERENCES

1. M.J. Pitkethly, Nanoparticles as building blocks, nanotoday, p. 36-42 (2003)
2. M.J. Pitkethly, Nanomaterials – the driving force, nanotoday, p. 20-29 (2004)
3. D.B. Williams and C.B. Carter, Transmission electron microscopy: a textbook for materials science, (Plenum Press, New York, 1996)
4. D.J. Smith, The realization of atomic resolution with the electron microscope, Rep. Prog. Phys. **60**, 1513-1580 (1997)
5. N.D. Browning, I. Arslan, P. Moeck, and T. Topuria, Atomic Resolution Scanning Transmission Electron Microscopy, phys. stat. sol. (b) **227** (2001) 229-245
6. E.D. James and N.D. Browning, Practical aspects of atomic resolution imaging and analysis in STEM, Ultramicroscopy **78** (1999) 125-139

7. P. Fraundorf, W. Qin, P. Moeck, and E. Mandell, Making sense of nanocrystal fringes, arXiv:cond-mat/0212281 v2 (2005), J. Appl. Phys., *accepted*
8. P. Moeck, B. Seipel, W. Qin, E. Mandell, and P. Fraundorf, Fringe fingerprinting and transmission electron goniometry, supporting image-based nanocrystallography in two and three dimensions, Proc. 9th World Multi-Congress on Systemics, Cybernetics and Informatics, Vol. **IX**, 249-254, July 10-13, 2005, Orlando, Florida, (Invited session "Nanotechnology: Materials, Metrology and Devices", Session organizer, P. Moeck)
9. P. Fraundorf, E. Mandell, W. Qin, and K. Cho, Fringe-covariance "fingerprinting" of nanoparticle lattice images, Microsc. Microanal. **10** (Suppl 2), 1262-1263 (2004), see also http://www.umsl.edu/~fraundor/covariances.html
10. W. Qin, Direct space nano(crystallography) via high-resolution Transmission Electron Microscopy, PhD thesis, University of Missouri-Rolla, (2000)
11. W. Qin and P. Fraundorf, Lattice parameters from direct-space images at two tilts, Ultramicroscopy **94**, 245-262 (2003) and arXiv:cond-mat/0001139
12. P. Moeck, W. Qin, and P.B. Fraundorf, Image-based nanocrystallography in future aberration corrected transmission electron microscopes, Mat. Res. Soc. Symp. Proc. Vol. **818** (2004) M11.3.1-M11.3.6
13. P. Moeck, B. Seipel, W. Qin, E. Mandell, and P. Fraundorf, Image-based nanocrystallography by means of tilt protocol/lattice-fringe fingerprinting in contemporary side-entry specimen goniometers, Microsc. Microanal. **11** (Suppl. 2) (2005) 632-633
14. P. Moeck, W. Qin, and P. Fraundorf, Towards 3D image-based nanocrystallography by means of transmission electron goniometry, Mat. Res. Soc. Symp. Proc. Vol. **839** (2005) P4.3.1-P4.3.6
15. P. Moeck, W. Qin, and P.B. Fraundorf, Image-based nanocrystallography by means of transmission electron goniometry, Nonlinear Analysis**,** 2005, *in press*
16. J.M. Cowley and S. Iijima, Electron microscope image contrast for thin crystals, Z. Naturforsch. **27a** (1992) 445-451
17. F.H. Li and D. Tang, Pseudo-weak-phase-object approximation in high-resolution electron microscopy, Acta Cryst. A **41** (1985) 376-382
18. F.H. Li, Image formation and image contrast in HREM, in D.L. Dorset et al. (eds.), Electron Crystallography, 29-35, Kluwer Academic Publ., 1997
19. M. Lentzen, B. Jahnen, C.L. Jia, A. Thust, K. Tillmann, and K. Urban, High-resolution imaging with an aberration-corrected transmission electron microscope, Ultramicroscopy **92** (2002) 233-242
20. B. Kabius, M. Haider, S. Uhlemann, E. Schwan, K. Urban, and H. Rose, First application of a spherical-aberration corrected transmission electron microscope in materials science, J. Electron. Microsc. **51** (Supplement) (2002) 551-558
21. S.J. Pennycook, A.R. Lupini, A. Kadavanic, J.R. McBride, S.J. Rosentahl, R.C. Puetter, A. Yahil, O.L. Krivanek, N. Dellby, P.D.L. Nellist, G. Duscher, L.C. Wang, and S.T. Pantelides, Aberration-corrected scanning transmission electron microscopy: the potential for nano- and interface science, Z. Metallkd. **94** (2003) 350-357
22. N. Tanaka, J. Yamasaki, S. Fuchi, and Y. Takeda, First Observation of $In_xGa_{1-x}As$ Quantum Dots in GaP by Spherical-Aberration-Corrected HRTEM in Comparison with ADF-STEM and Conventional HRTEM, Micros. Microanal. **10** (2004) 139-145
23. P. Schlossmacher, A. Thesen, and G. Benner. Picture perfect, European Semiconductor 27, No. 3 Mid-March (2005) 2-3, http://www.eurosemi.eu.com/front-end/features-full.php?id=5828 and EUROSEMI Bulletin, Issue **570** (January 26, 2005), p. 3
24. B. Freitag, S. Kujawa, P.M. Mul, J. Ringnalda, and P.C. Tiemeijer, Breaking the spherical and chromatic aberration barrier in transmission electron microscopy, Ultramicroscopy **102** (2005) 209-214
25. M. van der Stam, M. Stekelenburg, B. Freitag, D. Hubert, and J. Ringnalda, A New Aberration-Corrected Transmission Electron Microscope for a New Area, Microscopy and Microanalysis (The Americas Edition) **73**, 5-7, July 2005
26. S. Kujawa, B. Freitag, and D. Hubert, An Aberration Corrected (S)TEM Microscope for Nanoresearch, Microscopy Today **13**(4) pp. 16-18, July 2005
27. M.M.J. Tracy and J.M. Gibson, Variable coherence microscopy: a rich source of structural information from disordered systems, Acta Cryst. A **52** (1996) 212-220
28. P.M. Voyles. J.M. Gibson, and M.M.J. Tracy, Fluctuation microscopy: A probe of atomic correlations in disordered materials, J. Electron. Microsc. **49** (2000) 259-266
29. A. Kiesow, S. Strohkark, K. Löschner, A. Heilmann, A. Podlipensky, A. Abdolvand, and G. Seifert, App. Phys. Lett. **86** (2005) 153111-1-153111-3
30. E. Mandell, P. Fraundorf, and W. Qin, Measuring Local Thickness Through Small-Tilt Fringe Visibility, Microsc.

Microanal. **11**(Suppl. 2) (2005) 562-563
31. J.D.H. Donnay and W.A. O'Brien, Microscope goniometry, Ind. Engin. Chem. Anal. Ed. **17** (1945) 593-597
32. L.D. Marks, Dispersive equations for high resolution imaging and lattice fringe artifacts, Ultramicroscopy **12** (1994) 237-242
33. M. Koelsch, S. Cassaignon, C. Ta Thanh Minh, J.F. Guilemoles, and J.-P. Jolivet, Electrochemical Comparative Study of Titania (Anatase, Brookite and Rutile) Nanoparticles Synthesized in Aqueous Medium, Thin Solid Films **451/452** (2004) 86-92
34. U. Kolb, Electron Microscopy on Pigments*, in:* Industrial Applications of Electron Microscopy, ed. Z. R. Li, Marcel Dekker Inc. New York, 2003, p. 331-356
35. http://database.iem.ac.ru/mincryst/
36. http://Jmol.sourceforge.net
37. http://cst-www.nrl.navy.mil/lattice/index.html
38. http://www.reciprocalnet.org/
39. R.T. Downs and M. Hall-Wallace, The American Mineralogist crystal structure database, American Mineralogist **88** (2003) 247-250
40. http://rruff.geo.arizona.edu/AMS/amcsd.php
41. http://rruff.geo.arizona.edu/AMS/extra.php
42. F.H. Allen, The Cambridge Structural Database: a quarter of a million crystal structures and rising, Acta Cryst. B **58** (2002) 380-388
43. A. Le Bail, COD (Crystallography Open Database), Newsletter No. **29**, June 2003, 39-40, The International Union for Crystallography's Commission on Powder Diffraction, ISSN 1591-9552
44. http://www.crystallography.net
45. http://www.karmanaut.com/cosmo/player/
46. http://www.nanocrystal.research.pdx.edu/ncd
47. A.K. Boldyrew and W.W. Doliwo-Dobrowolsky, Bestimmungstabellen für Kristalle (Определитель Кристаллов), Vol. I, Part 1; W.W. Doliwo-Dobrowolsky and G.P. Preobraschensky, Vol. I, Part 2, Zentrales Wissenschaftlichers Institute der Geologie und Schürfung, Leningrad and Moscow, 1937 & 1939
48. R.W.G. Wyckoff, The Structure of Crystals, 2nd edition & Supplement for 1930-1934 to the 2nd edition, American Chemical Society Monograph Series 19 & 19a, Reinhold Publishing, 1931 & 1935
49. http://www.nanocrystal.research.pdx.edu/cod
50. http://checkcif.iucr.org/
51. Courtesy of Dr. Dedong Wu, AstraZeneca Pharmaceuticals LP, 1800 Concord Pike, Wilmington, DE 19850
52. J.R. Jinschek, H.A. Calderon, K.J. Batenburg, V. Radmilovic, and Ch. Kisielowski, Discrete Tomography of Ga and InGa Particles from HREM Image Simulation and Exit Wave Reconstruction, Mat. Res. Soc. Symp. Proc. **839** (2005) P4.5.1-P.4.5.6
53. B. Freitag, FEI Company presentation at "Microscopy and Microanalysis 2005", Honolulu, Hawaii, July 31-August 4, 2005, on-site demonstration of the FEI Titan 80-300 and private communications

♣ From the fringe fingerprinting of phase-contrast high resolution TEM images of 23 WC_{1-x} nanocrystals, space group $Fm\bar{3}m$, a = 0.425 nm, that were recorded at the University of Missouri's Philips EM430ST microscope on film and subsequently digitized, standard deviations from the means of fringe spacings and interfringe angles were less than 1.5 % and 1.3°, respectively.[10]

♣♣ While electrons are scattered elastically by the nucleolus of the atoms and inelastically at the valence and binding electrons, X-rays are scattered by the electron cloud as such. The atomic scattering factors are, therefore, quite different for both kinds of scattering, resulting in the intensity distribution of powder electron and X-ray diffraction curves being distinctly different as well. What we are interested in here is, however, not these differences, but the general idea of plots of probability of detecting scattering events versus spatial frequency.

♣♣♣ As far as spatial frequencies are concerned, the fringe fingerprint plot in Fig. 3b (for a point resolution of 0.07 nm) actually reaches further out in reciprocal space, i.e. reveals smaller lattice spacings, that the powder X-ray diffractogram in Fig. 6.

♣♣♣♣ Since its adoption in 1990 by the International Union of Crystallography as the standard file syntax for communicating crystallographic information between human beings and computers and between different kinds of software programs, CIF has become a crystallographic entity in its own right, see, e.g., I.D. Brown and B. McMahon, CIF: the computer language of crystallography, Acta Cryst. B **58** (2002) 317-324.

♣♣♣♣♣ This program can be downloaded for free at http://www.ccdc.cam.ac.uk/free_services/encifer/.

* pmoeck@pdx.edu; phone: 503 725 4227; fax: 503 887 0456; URL: www.physics.pdx.edu/~pmoeck